Chapter 3

Structure of Mesh Phases in Cationic Surfactant Systems with a Strongly Bound Counterion

3.1 Introduction

Mesh phases, made up of two dimensional (2-D) mesh-like surfactant aggregates, have been identified as one of the topological intermediates between the 2-D hexagonal phase formed by cylindrical micelles with uniform positive interfacial curvature and the lamellar phase consisting of bilayers with zero interfacial curvature [1]. They are known to occur in a wide variety of amphiphilic systems ranging from anhydrous soap melts, ionic and nonionic single-chained surfactants to block copolymers, but they do not seem to be as prevalent as the bicontinuous cubic phases, which also usually occur in between the hexagonal and lamellar phases [2]. Two types of mesh phases have been identified; the random mesh phase, where inter-mesh correlations are absent, and the intermediate mesh phase, where the mesh-like aggregates lock into a 3-D lattice.

The phase behaviour of the ternary system consisting of cetyltrimethylammonium bromide (CTAB), 3-sodium-2-hydroxy naphthoate (SHN) and water has been described in the previous chapter and also reported in the literature [3, 4]. In this system a transition from a random mesh phase to the lamellar phase was found to occur through an intermediate mesh phase with increasing surfactant concentration at lower temperatures. The motivation for the work described in this chapter was to find the structure of the intermediate phase which was tentatively identified as a centred rectangular phase (*R*) earlier [4]. In the present chapter, a structure is proposed for

the intermediate mesh phase based on x-ray diffraction data and polarizing optical microscopy observations. In the CTAB-SHN system, consisting of oppositely charged molecules, an increase in the surfactant concentration is accompanied by a corresponding increase in the ionic strength due to the released Br^- and Na^+ counterions. Hence the effects of salt and surfactant concentration on the phase behavior cannot be separated. Therefore, we have studied the phase behavior of the surfactant CTAHN, which is formed by the complexation of CTAB and SHN, as a function of NaBr concentration. In order to understand the influence of the chain length of the surfactant molecule on inducing the mesh phase, we also discuss the dodecyltrimethylammonium bromide(DTAB)- SHN - water system whose phase behaviour has been described in the previous chapter (Fig. 2.17).

Section 3.2 gives a short review of earlier studies on mesh phases. In section 3.3, a brief outline of the experimental techniques used is given, and our results are described in section 3.4. X-ray diffraction data from oriented samples of CTAB-SHN system in the intermediate phase show the existence of a 3-D lattice with rhombohedral symmetry. The intermediate mesh phase is also recovered in the CTAHN-water system at high NaBr concentrations. The intermediate mesh phase is absent in DTAB-SHN system and only the random mesh phase is observed over a wide range of surfactant concentration (ϕ_s). In section 3.5 a structural model for the mesh phases is presented. The random mesh phase is found to consists of a stack of 2-D network of rod-like aggregates, with no long-range positional correlations along their normal. These aggregates are regularly stacked to from a 3-D lattice in the intermediate phase. The diameter of the rod-like segments was estimated from the data and is found to be consistent with the length of the surfactant molecule. The average mesh size is found to increase with ϕ_s in the random mesh phase and the transition to the intermediate mesh phase occurs when it is of the order of 1.4 times the lamellar periodicity d. In the DTAB-SHN system, on the other hand, the average mesh size decreases with ϕ_s; which might me a reason for the absence of the intermediate phase in this system. Most of the samples in the intermediate phase also give rather broad x-ray diffraction peaks in the small angle region, corresponding to average periodicities of around 25nm. These peaks seem to be arising from some nodule-like structures seen in freeze-fracture electron micrographs of some samples in the intermediate phase. Conclusions that can be drawn from these studies are given in section 3.6.
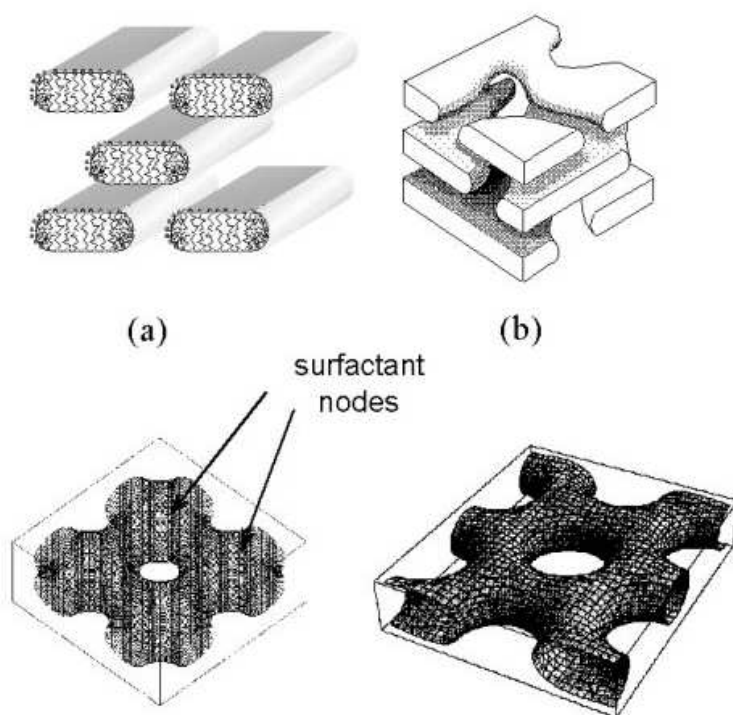
Figure 3.1: Schematic diagram of (a) centred rectangular lattice made up of ribbon-like aggregates, (b) a random mesh phase, (c) a square mesh layer and (d) a hexagonal mesh layer [9].

3.2 Earlier studies

The random mesh phase has been observed in some binary and ternary surfactant-water mixtures. It can be distinguished from the conventional lamellar phase by the presence of structural inhomogeneities in the plane of the bilayer, revealed by x-ray and neutron scattering studies [5, 6]. The occurrence of mesh-like aggregates in this phase has also been indicated by nuclear magnetic resonance (NMR) and electrical conductivity studies [7, 8] which show the presence of nonuniform interfacial curvature and significant out-of-plane mobility of the counter ions, respectively. An increase in surfactant concentration (ϕ_s) or a decrease in temperature (T) results, in some cases, in the development of out-of-plane positional correlations of the mesh-like aggregates, leading to the formation of intermediate mesh phases with 3-D tetragonal or rhombohedral lattices [9]. Though there are reports of intermediate phases with non-cubic bicontinuous structures in some systems [5, 10], the mesh phases seem to be more commonly observed after the cubic phases. The structure of the mesh phases has been characterized by x-ray diffraction and the nonuniform interfacial cur-

vature of the aggregates forming intermediate mesh phases has been established through deuterium NMR studies [11]. In binary mixtures of ionic surfactants and water, the mesh phase usually occurs only over a narrow region in the phase diagram, although by adding long-chain alcohols and by tuning the ratio of the surfactant to alcohol its extent could be increased [6].

Mesh phases have also been seen in nonionic surfactant-water mixtures. Here a first order transition from a random mesh to the lamellar phase has been observed on increasing the alkyl chain length. It was also found that the intermediate mesh phase could be stabilized over a large range of ϕ_s by increasing the chain length of the surfactant [11, 12, 13, 14]. Besides the length of the alkyl chain, the counter ion of the amphiphile is also known to influence the stability of the mesh phases in some binary ionic surfactant-water mixtures [15]. A transition from a random mesh phase to the intermediate mesh phase with increasing ϕ_s has also been observed in an ionic surfactant-water system [16]. Here the intermediate mesh phase is found to be destabilized by additives, such as salt and alcohol, by bulky counter ions, and by amphiphiles with shorter alkyl chains [2]. A schematic diagram of the two types of mesh phases is shown in figure 3.1.

3.3   Experimental

CTAHN was prepared by mixing equimolar ratios of sodium hydroxynaphthoate (SHN) dissolved in methylisobutyl ketone (MIBK) and CTAB in water. The CTAHN complex obtained was extracted by vacuum distillation and subsequently dried in a rotary evaporator [17]. The structures of all the chemicals have been shown in the previous chapter. Details of sample preparation and experimental techniques used to identify the phases are the same as those described in chapter 2. The parameters ϕ_s and α have been defined as in the previous chapter.

Small angle x-ray scattering experiments on unoriented samples, covering a q-range from 0.05 to 1.0 nm^{-1}, was carried out in collaboration with R. Ganapathy at the department of physics, Indian Institute of Science, Bangalore, India. Freeze fracture electron microscopy experiments on some of the samples were carried out by J. Bellare, at the Department of Chemical Engineering, Indian Institute of Technology, Bombay, India.
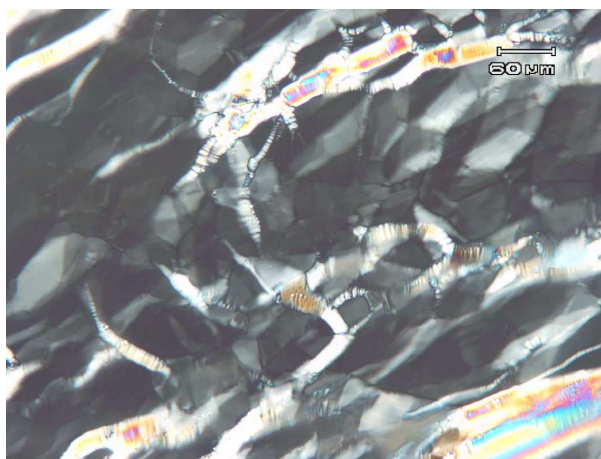
Figure 3.2: Optical microscopy texture of CTB-SHN-water system at $\alpha = 1$, $\phi_s = 60$ and T = 60°C. Both the oily streak and mosaic textures are seen indicating the coexistence of L_α^D and intermediate phases.

3.4   Results

3.4.1   CTAB-SHN-water system

The phase behaviour of this system has been described in detail in the previous chapter. Some important observations related to mesh phases are, however, restated here. Upon cooling the lamellar phase at $\alpha = 1$, $\phi_s = 60$, the mosaic texture characteristics of 2D ordered phases is observed to coexist with oily streak texture under microscope over a few °C (Fig. 3.2). It indicates a first order phase transition between these two phases. It is sometimes possible to obtain partial alignment of the samples in the lamellar phase with the bilayers parallel to the glass plates. Interestingly, these "homeotropic" regions persist even after cooling the samples down to the intermediate phase (Fig. 3.3). The diffraction pattern of the intermediate phase at $\phi_s = 60$ consists of about 6 peaks in the small angle region. The diffraction pattern of a partially oriented sample is shown in figure 3.4 and a typical pattern obtained from unoriented samples is shown in figure 2.10. Diffraction patterns of this phase for all compositions are qualitatively similar, with only slight changes in the spacings with changes in α, ϕ_s and T.
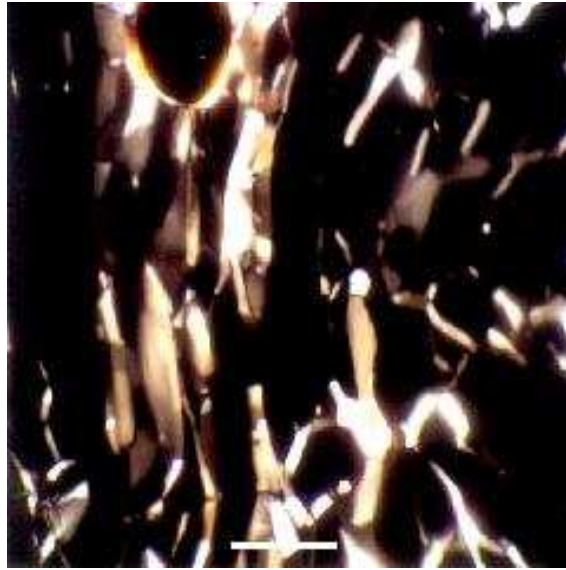
Figure 3.3: Optical microscopy texture of the intermediate phase in CTAB-SHN-water system, showing dark regions where the optic axis is aligned normal to the substrates ($\alpha = 1$, $\phi_s = 60$, T = 30°C) [3].
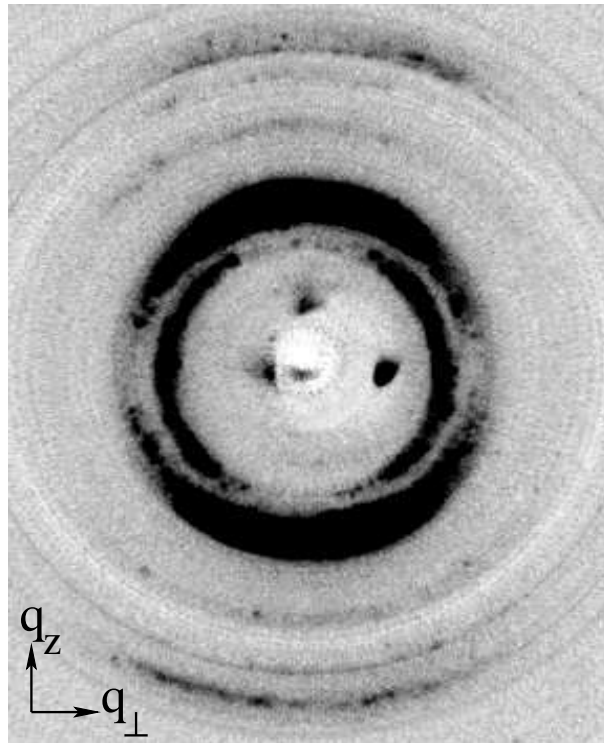

q_z

$q_\perp$

Figure 3.4: X-ray diffraction pattern of a partially aligned sample in the intermediate phase at $\alpha = 1$, $\phi_s = 60$ and T = 30°C.
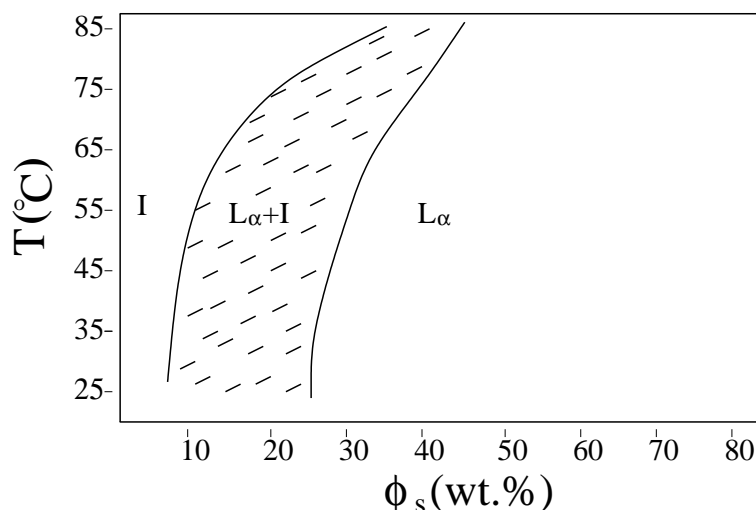
Figure 3.5: Phase diagram of the CTAHN-water system. The shaded regions in all the phase diagrams correspond to multiphase regions.

3.4.2 CTAHN-water system

Microscopy observations indicate that CTAHN forms a lamellar phase over a large range of ϕ_s between 25 and 80 (Fig. 3.5). The diffraction pattern at $\phi_s = 60$ consists of 2 peaks in the small angle region with their q values in the ratio 1:2 corresponding to a lamellar structure. However, the diffuse peak arising due to the in-plane structure of the bilayers was found to be absent at all surfactant concentrations up to 60 °C. At higher temperatures the lamellar phase is retained at all surfactant concentrations, with the lamellar periodicity decreasing slightly with increasing temperature.

In some samples diffuse peaks are observed along $q_\perp$ in addition to the lamellar reflections at $T > 60$ °C (Fig. 3.6) indicating the presence of a random mesh phase. The position of these peaks do not change significantly up to 80 °C. On cooling, they disappear below 60°C.

3.4.3 CTAHN-NaBr-water system

The effect of NaBr on the phase behavior of CTAHN was studied over a large range of surfactant concentration. The results are summarized in figures 3.7 and 3.8. At salt concentrations $\rho < 0.75$ M a multiphase region is observed for $\phi_s < 65$, which was not probed in detail to identify the coexisting phases. At higher values of ρ a random mesh phase is observed for this range of
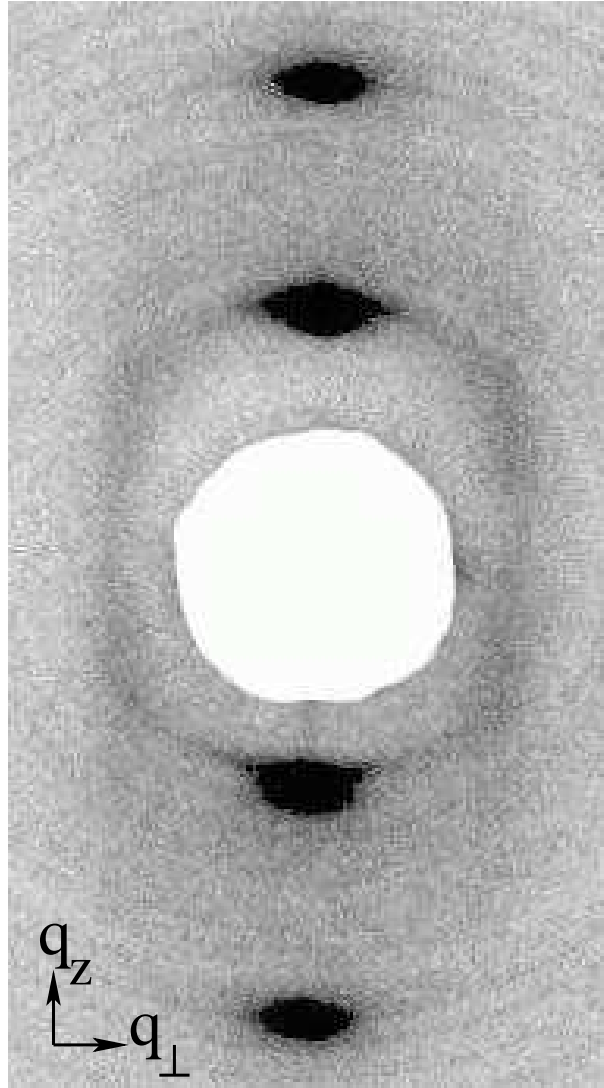
Figure 3.6: Diffraction pattern of the random mesh phase observed in the CTAHN-water system at $\phi_s = 60$, T = 70 °C. The shift of the diffuse peaks from the $q_\perp$ axis indicates the presence of transbilayer correlations of the in-plane structure.
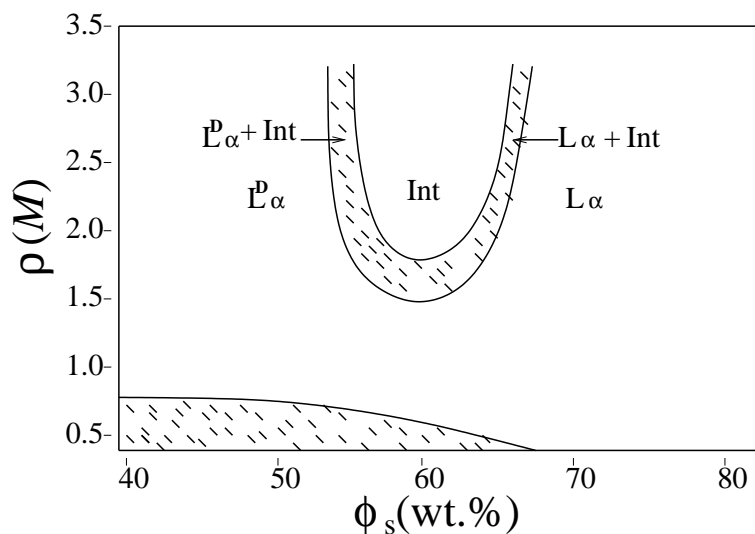
Figure 3.7: Phase diagram of the CTAHN-NaBr system at T = 30°C in the ρ (=[NaBr]) - ϕ_s plane.

ϕ_s. At $\phi_s = 40$ and $\rho = 1.0$ M this phase has a lamellar periodicity of 6.92 nm at 30°C (Table 3.1). The diffuse peak is found to shift to smaller values of q with increasing ρ. At $\phi_s = 60$ the lamellar periodicity is 4.60 nm for $\rho = 0.75$ M, and a diffuse peak is seen at 6.70 nm. With further increase in the salt concentration ($1 < \rho < 1.3$), the lamellar periodicity remains the same, but the diffuse peak is no longer present even at higher temperatures. At higher values of ρ (> 1.3 M) microscopy observations indicate the formation of the intermediate phase for a range of ϕ_s around 60. Diffraction pattern of this phase consists of a few sharp peaks in the small angle region as in figure 2.10.

For $\phi_s > 70$ a regular lamellar phase is obtained at all salt concentrations, and the lamellar periodicity remains the same as that observed in the absence of salt. At lower values of ρ the random mesh phase is transformed into a lamellar phase on increasing ϕ_s.

SAXS studies of the intermediate phase show the presence of additional peaks in the small angle region of the diffraction pattern, which disappear on heating the sample to the random mesh phase (Fig. 3.9). Although many of these peaks could not be consistently reproduced, many samples of the same composition revealed a reproducible peak at ∼ 25nm. To probe the structure further at these length scales, freeze fracture electron microscopy observations were carried out on these samples. These indicate a fine mesh like structure in the plane of the bilayers in the intermediate phase (Fig. 3.10). This structure does not seem to be correlated over long distances,
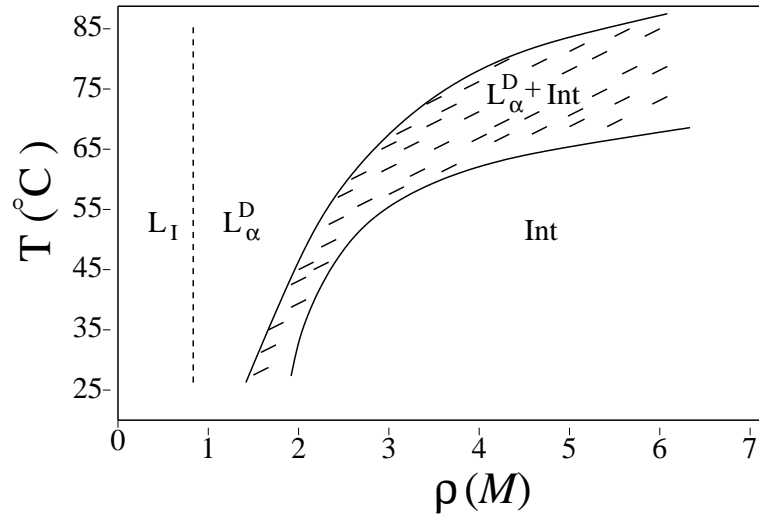
Figure 3.8: Phase diagram of the CTAHN-NaBr system in the T - ρ plane at ϕ_s = 60. L_I denotes multiphase region.

Table 3.1: The lamellar periodicity (d) and the average defect separation (d_d) in the lamellar phase of CTAHN-NaBr-water at a few values of ϕ_s and ρ=[NaBr].

ϕ_s	ρ	d(nm)	d_d(nm)
40	0	7.9	-
	1	6.92	7.04
	1.5	6.16	7.17
	4	5.63	7.58
50	0	6.24	-
	1	5.76	6.91
60	0	5.0	-
	0.75	4.60	6.70
	1	4.63	-

63
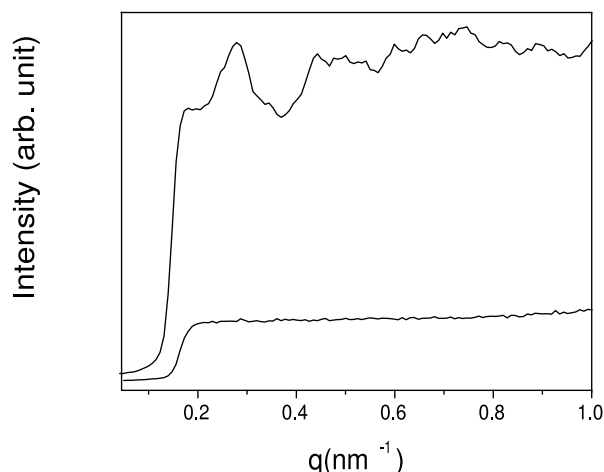
Figure 3.9: Small angle x-ray diffraction pattern of the CTAHN-NaBr-water system at $\phi_s = 60$, [NaBr] = 2.6 M and T = 30 °C (upper curve). The diffraction pattern in the higher temperature lamellar phase is shown for comparison (lower curve).

but shows short-range periodicity of 5 - 7 nm (Fig. 3.11). In addition to the mesh like structure, nodule like structures with an average size of around 30 nm were observed in some samples in the intermediate phase (Fig. 3.12).

3.4.4 DTAB-SHN-water system

The detailed phase diagram of this system has been shown in chapter 2. It forms the L_α^D phase over the composition range studied, with the average defect separation decreasing with increasing ϕ_s. This trend is opposite to that seen in the CTAB-SHN system. Figure 3.13 shows the swelling behavior of the L_α^D phase in the DTAB-SHN-water system. It is found to be well described by the relation, $d \sim \phi_v^{-s}$, with $s = 0.63$, where ϕ_v is the volume fraction of the non-aqueous components, estimated from ϕ_s using the densities of these components.

3.5 Discussion

3.5.1 Structure of the mesh phases

3.5.1.1 CTAB-SHN-water

The microscopy observation that homeotropically aligned regions in the lamellar phase remain unaltered in the lower temperature intermediate phase indicates that the latter is also optically

64
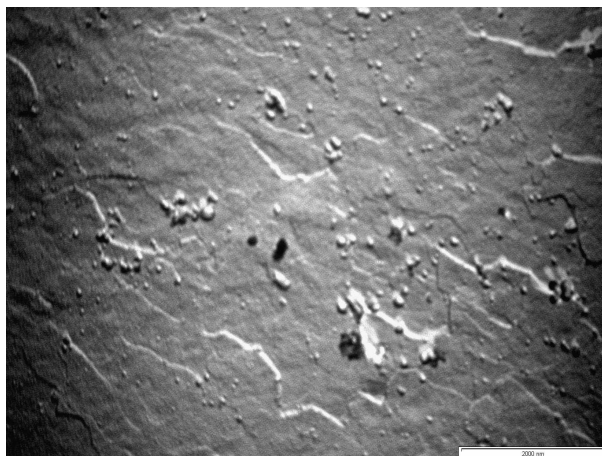
Figure 3.10: Freeze fracture electron micrograph of the intermediate phase of the CTAHN-NaBr-water system at $\phi_s = 60$, [NaBr] = 2.6 M and T = 30 °C. The scale bar corresponds to 2000nm.

Figure 3.11: Part of fig. 3.10 enlarged to show the fine mesh-like structure in the plane of the bilayer.
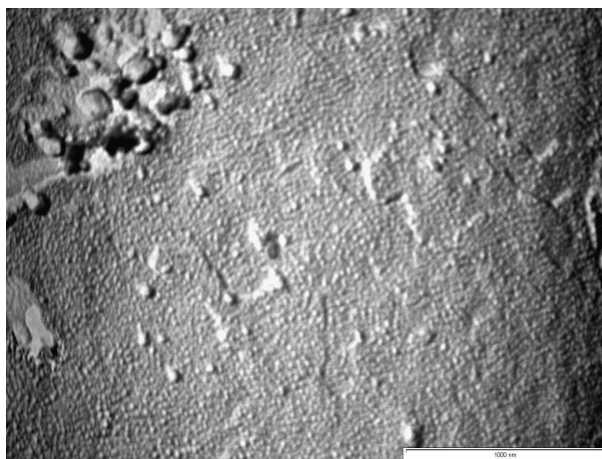
Figure 3.12: Freeze fracture electron micrograph of the intermediate phase showing nodule-like structures in the plane of the bilayer in the CTAHN-NaBr-water system at $\phi_s = 60$, [NaBr] = 2.6 M and T = 30 °C. The scale bar corresponds to 1000nm.

uniaxial. This reduces the possible structures of this phase to either tetragonal or hexagonal, similar to the structures of intermediate phases seen in some ionic and nonionic surfactant systems as well as in some block copolymers. The diffraction pattern of this phase contains one very strong reflection, whose spacing is very close to that of the peak in the higher temperature random mesh phase. It also smoothly continues into the lamellar peak of the random mesh phase seen at lower values of ϕ_s. These observations suggest that the intermediate phase also consists of mesh-like aggregates, with the additional peaks arising from the locking-in of the mesh into a 3-D lattice.

The reflections from the intermediate phase could be indexed on a 2-D rectangular lattice corresponding to the space group *cmm* with lattice parameters $a = 12.9$ nm and $b = 5.72$ nm. Indeed earlier in reference [4] a centred rectangular lattice was assigned to this phase. However, in such a structure, usually formed by ribbon-like aggregates, the ribbons have to align with their long axes normal to the plates to give rise to the dark regions observed in the microscopy texture. This is highly unlikely since ribbon and the closely related hexagonal phases usually align with their constituent long aggregates parallel to the bounding surfaces. Hence the ribbon phase can be ruled out as a possible structure of the intermediate phase.

The reflections obtained at $\alpha = 0.67$ and $\phi_s = 60$ in the intermediate phase cannot be indexed on to a 3-D tetragonal lattice. They, however, can be indexed on to a 3-D hexagonal lattice corresponding to the space group $R\bar{3}m$. Two indexing schemes are possible with the lattice parameters
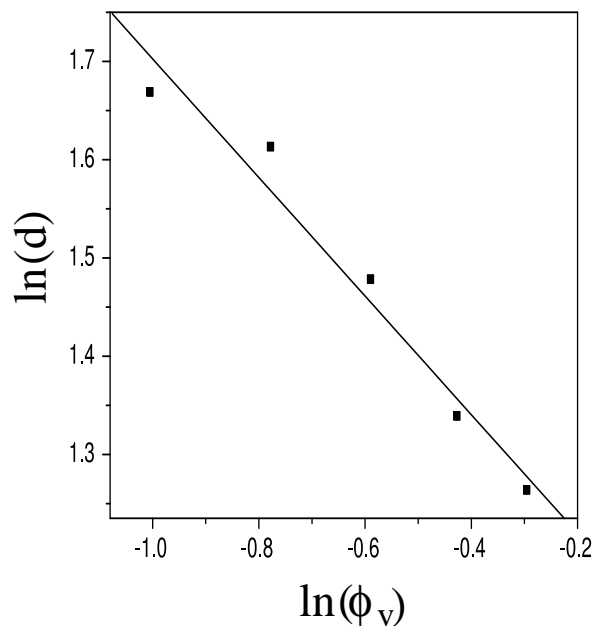
Figure 3.13: Variation of the *d*-spacing of the L_α^D phase with surfactant volume fraction (ϕ_v) in the DTAB-SHN-water system at $\alpha = 1$ and T = 30 °C.

$a = 7.41$ nm and $c = 14.64$ nm or $a = 11.4$ nm and $c = 14.6$ nm (Table 3.2). It is interesting to note that the diffraction data consisting of 9 reflections for the rhombohedral mesh phase studied by Funari et al. [12], could also be indexed using these two schemes. However, in the present case we can use the additional information from the partially oriented patterns (Fig. 3.4) to rule out the second possibility, according to which some of the reflections have $l = 0$. These reflections should, therefore, fall on the $q_\perp$ axis, which is not the case. Hence we take the structure to correspond to scheme 1. This has the additional feature that the value of the lattice parameter *a* is the continuation of the position of the diffuse peak seen in the random mesh phase. The structure of the intermediate mesh phase in the nonionic system, proposed in reference [12], also corresponds to this scheme of indexation.

The intermediate phase transforms into the random mesh phase at 75 °C on heating, with the lamellar periodicity comparable to the spacing of the (003) reflection of the intermediate phase. As mentioned earlier, this observation suggests that the intermediate phase has a layered structure and is closely related to the random mesh phase. Such layered structures with a rhombohedral symmetry have been observed in many surfactant systems (Fig. 3.14). These consist of a 2-D network of rod-like aggregates interconnected to form a hexagonal mesh. Each unit cell of the 3-D
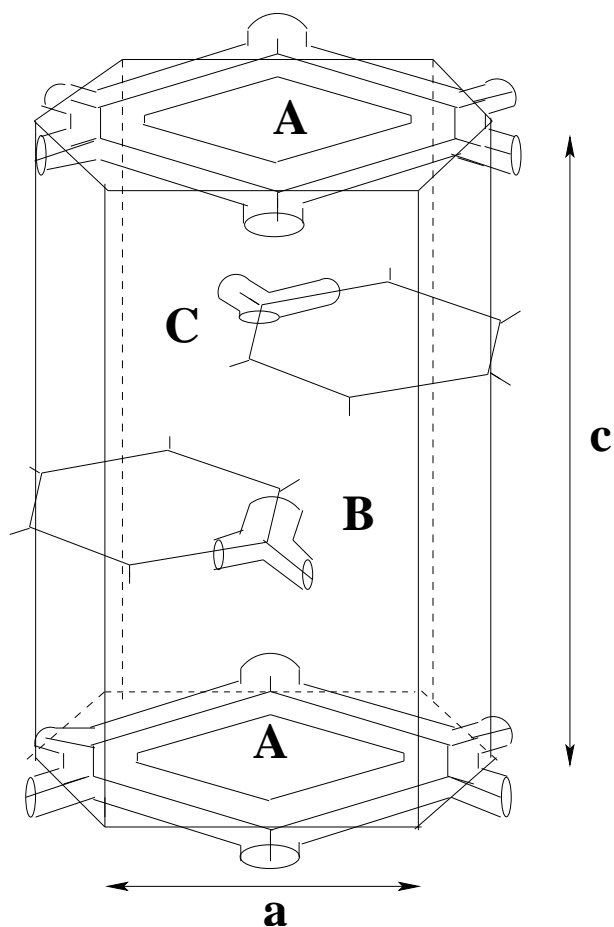
Figure 3.14: Model for the intermediate phase showing the unit cell of the hexagonal mesh structure.

hexagonal lattice has a three-layer stacking (ABC) of these meshes. Increasing the temperature would result in the loss of out-of-plane correlations, leading to a random mesh phase.

Diffraction patterns of the intermediate phase, through out the composition range where it is stable, could be indexed on the same lattice, with the lattice parameters varying with α, ϕ_s and the temperature (Table 3.3). Table 3.3 also gives the variation of the ratio γ of the in-plane periodicity to the stacking periodicity with ϕ_s and α in the intermediate phase; corresponding data for the random mesh phase are given in table 3.5 for $\alpha = 1$. (In the intermediate phase $\gamma = 3a/c$, and in the random mesh phase $\gamma = d_d/d$.) As can be seen from these tables, γ increases gradually with increasing ϕ_s in the random mesh phase and the transition to the intermediate mesh phase occurs at $\gamma \sim 1.4$, consistent with observations on other surfactant systems [15, 16, 18]. The modulated part of the interaction potential between the planar surfaces (arising due to the structural inhomogeneity

Table 3.2: X-ray diffraction data from the intermediate phase of the CTAB-SHN-water system at $\alpha = 0.67$ and $\phi_s = 60$, indexed on a rhombohedral (R$\bar{3}$m) lattice. The calculated spacings (d_{calc}) are obtained from the relation, $(1/d)^2 = (4/3)(h^2 + hk + k^2)/a^2 + l^2/c^2$ with the condition -h+k+l = 3n, where n is an integer. Two schemes of indexing are presented corresponding to unit cell parameters $a = 7.4$ nm, $c = 14.6$ nm, and $a = 11.4$ nm, $c = 14.6$ nm (d_{obs} are taken from ref.[3]).

	Scheme 1		Scheme 2		
d_{obs}(nm)	d_{calc}(nm)	h k l	d_{calc}(nm)	h k l	Intensity
6.61	6.61	(101)	6.61	(110)	s
4.88	4.88	(003)	4.88	(003)	vs
3.31	3.28	(104)	3.31	(220)	w
2.73	2.72	(015)	2.73	(223)	w
2.44	2.44	(006)	2.44	(006)	w

Table 3.3: Lattice parameters of the intermediate rhombohedral mesh phase of the CTAB-SHN-water system at a few different values of α and ϕ_s at T = 30 °C [4]. $\gamma = 3a/c$ is the ratio of the in-plane and out-of-plane periodicities. $r_m^{(3)}$ and $r_m^{(6)}$ are the values of the micellar radius estimated from models A and B, respectively. a and c are the lattice parameters of the 3-D hexagonal lattice.

α	ϕ_s	ϕ_v	a(nm)	c(nm)	$r_m^{(3)}$	$r_m^{(6)}$	γ
0.4	60	58.2	8.08	14.25	2.09	1.66	1.7
0.67	55	52.4	7.82	15.87	2.06	1.65	1.47
	60	57.3	7.41	14.64	2.03	1.62	1.52
	70	65.0	6.71	14.37	2.07	1.67	1.44
1	55	51.7	7.57	16.53	2.07	1.65	1.37
	60	56.5	7.26	15.21	2.03	1.63	1.43
	70	65.6	6.32	12.36	1.86	1.50	1.53

in the plane) decays exponentially with a decay length of the order of the in-plane periodicity [19]. Only when the separation between the layers of random meshes is low compared to the in-plane periodicity, the interaction potential is strong enough to lock the meshes to give rise to the 3-D ordered phase.

3.5.1.2 CTAHN-water

The lamellar phase found in this system at lower temperatures seems to consist of regular bilayers, as indicated by the absence of diffuse peaks in the direction normal to the lamellar peaks. The bilayer thickness estimated from the diffraction data ($\delta \approx 3.0$ nm) is also consistent with such a structure. The decrease in the lamellar periodicity at higher temperatures ($T > 60°C$) and the observation of a diffuse peak in some samples at these temperatures suggest the formation of a random mesh phase on heating.

3.5.1.3 CTAHN-NaBr-water

The intermediate phase here is very similar to that in the CTAB-SHN-water system, and can again be indexed on to a 3-D hexagonal lattice corresponding to the space group $R\bar{3}m$ (Table 3.4). Though a transition from the random mesh to the intermediate phase occurs on addition of NaBr to the CTAHN-water system at $\phi_s = 60$, further addition of salt does not lead to a regular lamellar phase. Salt is known to destabilize the intermediate mesh phase [2], but in the present system we observe a transition from a random mesh to the intermediate phase in the presence of NaBr. However such a transition could not be obtained by replacing NaBr with NaCl indicating the importance of counterion specific interactions.

3.5.2 Modeling the mesh phases

Two possible types of aggregates have been proposed for the hexagonal intermediate mesh phases in the literature, which can be described as networks of rod-like segments [11, 12, 13, 18]. In the first one (model A) three rods meet at each node, giving rise to a 2-D hexagonal lattice of pores (Fig. 3.15). In the other structure (model B) six rods meet at each node, and the nodes themselves are arranged on a 2-D hexagonal lattice (Fig. 3.16). In order to differentiate between these two

Table 3.4: X-ray diffraction peaks of CTAHN-NaBr-water system at $\rho = 2.6$ M and $\phi_s = 60$, indexed on an rhombohedral (R$\bar{3}$m) lattice.

d_{exp}(nm)	d_{calc}(nm)	plane	intensity
5.95	5.95	(101)	vs
4.75	4.74	(012)	-
4.55	4.55	(003)	vvs
3.02	3.03	(104)	w
2.51	2.52	(015)	vw
2.25	2.27	(006)	w

possibilities we have estimated the radius r_m of the rod-like segments from the experimental data. Since r_m can be expected to be comparable to the molecular length, the values obtained from the models can be used to choose between the two possible structures. This analysis will also show how well the aggregates in the system can be described as mesh-like, instead of as bilayers containing a regular arrangement of monodisperse pores, since in the latter case the estimated values of r_m will be much larger than the radius of the cylindrical micelles. We use the rod and box models of these structures discussed in references [11, 13]. As mentioned there, the values of the model parameters do not change significantly on using more sophisticated models for the mesh-like aggregates. We have also extended this analysis to the random mesh phase, assuming that the average structure of the mesh in this phase is similar to that in the intermediate phase.

We find that the values of r_m obtained from model A are comparable to the values of the micellar radius of similar systems reported in the literature [20, 21]; whereas values obtained from model B are much smaller. Thus it is clear that the aggregate in this system can be satisfactorily described as a mesh, with three rod-like segments meeting at each node, and not as a bilayer containing pores. In the case of single component systems it is also possible to estimate the interface area per molecule from both these models, which in turn can be used to test the models. Such an analysis cannot be used in the present mixed surfactant system, since the concentration of the two species need not be uniform in the mesh. We have also not considered other bicontinuous structures of the intermediate phase discussed in reference [13], which will give smaller, and, therefore, even more

unrealistic values of r_m.

3.5.2.1 Intermediate mesh phase

In model A the structure of the intermediate mesh phase corresponds to a 3-layer stacking of the mesh-like aggregates as shown in figure 3.14. The length of each cylindrical segment l can be expressed in terms of the lattice parameter a and the micellar radius r_m as [11]

$$l = \frac{1}{\sqrt{3}}(a - 2r_m). \tag{3.1}$$

The volume occupied by the surfactant, expressed in terms of the micellar radius, the only unknown parameter in the model, is equated to the volume estimated from the surfactant weight fraction and unit cell volume. This yields the cubic equation,

$$4(2 - \pi)r_m^3 + 2\pi a r_m^2 - a^2 d\phi_v = 0, \tag{3.2}$$

where $d = c/3$ and ϕ_v is the volume fraction of the surfactant. Out of the 3 roots obtained for the cubic equation, only one turns out to be reasonable with the other two being either negative or unrealistically large. Values of the micellar radius in the intermediate phase obtained at different surfactant concentrations of CTAB-SHN are listed in table 3.3.

The corresponding expressions for model B are:

$$l = a - 2\sqrt{3}r_m, \tag{3.3}$$

and

$$12(2 - \pi)r_m^3 + 2\sqrt{3}\pi a r_m^2 - a^2 d\phi_v = 0 \tag{3.4}$$

The values of r_m obtained from this model are also given in table 3.3.

As can be seen from table 3.3 values of r_m obtained from model A are much higher than those from model B. The former values are also comparable to those quoted in the literature for cylindrical CTAB micelles which varies between 1.9 to 2.2 nm [21]. On the other hand, values
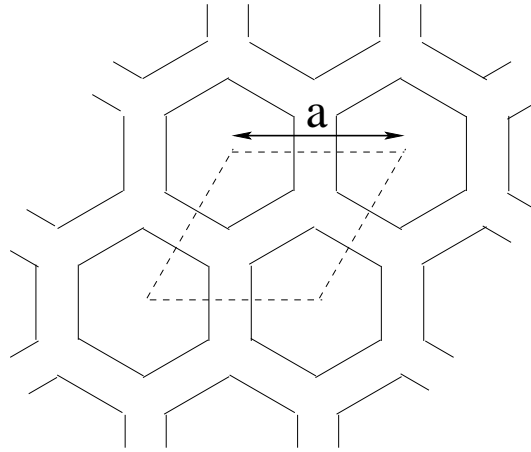
72

Figure 3.15: Schematic of the 3 coordinated mesh in the hexagonal intermediate phase.

obtained from model B are too low to be realistic. Thus we can rule out model B as a possible structure of the intermediate mesh phase in the present system.

As discussed earlier, the formation of mesh phases involves the creation of branch points or nodes where the three rod-like micelles meet. In the structure that has been proposed the rods meeting at a branch point are confined to a plane. It can be expected that such cylindrical rod-like aggregates would form bicontinuous structures or a 3-D mesh rather than a 2-D mesh. Though non-cubic bicontinuous structures have been proposed in some systems, intermediate mesh phases were found to be more consistent with the experimental observations [18]. The formation of a 2-D mesh also suggests that the cross section of the rods is probably better described as elliptical rather than circular, favoring them to lie in a plane. In the present model, the elliptical cross section of the rod has not been taken into account since it would increase the number of unknown parameters. However the reasonable values obtained for the micellar radius suggests that the eccentricity of the ellipse is negligible.

3.5.2.2   Random mesh phase

If the random mesh phase consists of similar aggregates as the intermediate phase, albeit without long range correlation, then the above analysis should hold good in this phase also. With this in mind we have estimated the micellar radius r_m using the above expressions, with the lattice parameter a replaced by the average separation of the defects d_d. As in the case of the intermediate phase
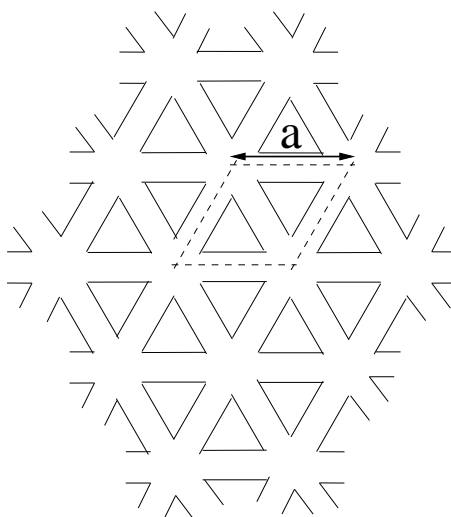
Figure 3.16: Schematic of the 6 coordinated mesh in the hexagonal intermediate phase.

Table 3.5: Variation of the lamellar periodicity (d) and the average in-plane periodicity (d_d) with ϕ_s in the CTAB-SHN-water system at $\alpha = 1$ and T = 30 °C. r_m is the micellar radius estimated from model A, discussed in the text. $\gamma = d_d/d$.

ϕ_s	d(nm)	d_d(nm)	r_m	γ
30	9.6	5.93	1.88	0.69
40	7.17	6.93	2.0	0.97
50	5.85	7.45	2.08	1.27

only model A gives reasonable values of r_m (Table 3.5). It is interesting that these values are very close to those obtained for the intermediate phase, confirming the similarity of the aggregates in the two phases. On increasing the surfactant content r_m increases slightly as seen in the hexagonal phase of many systems [22].

3.5.3   Influence of alkyl chain length

In the DTAB-SHN system the average separation between the defects decreases on increasing ϕ_s. The random mesh phase of DTAB-SHN was also modeled based on the structure proposed for that of CTAB-SHN. The radius of the cylinders estimated from the model is found to decrease slightly on increasing ϕ_s (Table 3.6). The estimated radius of DTAB micelles is also comparable to the values quoted in the literature for the length of the surfactant molecule. The absence of

Table 3.6: Variation of the lamellar periodicity (d) and the average in-plane periodicity (d_d) in the DTAB-SHN-water system at $\alpha = 1$ and T = 30 °C. r_m is the micellar radius of DTAB-SHN estimated from model A. $\gamma = d_d/d$.

ϕ_s	d(nm)	d_d(nm)	r_m	γ
60	4.38	5.87	1.77	1.34
70	3.81	5.23	1.70	1.37
80	3.54	4.42	1.65	1.25

the intermediate phase in the DTAB-SHN-water system is consistent with observations in some nonionic surfactant systems, where decreasing the alkyl chain length destabilizes the ordered mesh phase. In the present system this might be related to the decrease in γ with increasing surfactant content. The modulated part of the interaction potential is not strong enough to lock the meshes due to the comparable values of the in-plane and stacking periodicities.

The swelling behavior of the L_α^D phase in this system, with an exponent $s = 0.63$ (Fig. 3.13) is also consistent with the presence of mesh-like aggregates in this phase [1, 11]. In the L_α phase $s \sim 1.0$ and in the hexagonal phase it is ~ 0.5. The intermediate value of s found here reflects a micellar morphology in between a cylinder and a bilayer.

3.5.4   Large scale structures in the intermediate mesh phase

The fine mesh-like pattern observed in the freeze fracture studies with a short-range periodicity of 5 to 7 nm is consistent with the structure proposed for the intermediate phase in the present system. Similar fine structures have been revealed in TEM studies of the intermediate phases in some block copolymers [23]. The nodule-like structures observed in some samples with average separation ~ 30 nm might be due to the presence of pores in the bilayer. They could also arise from a dispersion of vesicles coexisting with the intermediate phase. It is very likely that these structures are responsible for the scattering in the small angle region observed from this phase. Since these structures are not seen in all the samples they are likely to be metastable. Further studies are required to probe these structures in more detail.

3.6 Conclusion

In conclusion, we have determined the structure of the intermediate phase observed between a random mesh and lamellar phases in a mixed ionic surfactant system formed by CTAB and SHN. It is found to consist of a three-layer stacking of 2-D network of rod-like micelles, corresponding to the space group $R\bar{3}m$. The aggregate morphology is identical in the random mesh phase, which occurs at lower surfactant concentrations, although the long-range positional order present in the intermediate phase is absent in this case. On examining the influence of salt on the phase behavior of the mixed surfactant system, we find that similar phases can be obtained in the CTAB-SHN-water and the CTAHN-NaBr-water systems. The intermediate phase is lost on decreasing the alkyl chain length of the surfactant, consistent with earlier observations. Somewhat surprisingly, the dependence of the mesh size in the random mesh phase on the surfactant concentration shows opposite trends in the CTAB and DTAB mixtures. At present we do not understand the reasons for this difference, but it is likely that the appearance of intermediate phase in CTAB-SHN and its absence in DTAB-SHN is related to this. These observations show the rich phase behavior of concentrated solutions of mixed ionic surfactant systems, which hitherto have mainly been studied in the dilute limit.

Bibliography

[1] S. T. Hyde *Colloq. de Phys*. **C7**, 209 (1990).

[2] M. C. Holmes and M. S. Leaver in *Bicontinuous Liquid Crystal, Intermediate Phases* ; Lynch, M. L.; Spicer, P. T. Eds.; Taylor & Francis: NW, 2005; pp 15-39.

[3] R. Krishnaswamy, S. K. Ghosh, S. Lakshmanan, V. A. Raghunathan and A. K. Sood *Langmuir* **21**, 10439 (2005).

[4] R. Krishnaswamy, Ph. D Thesis: *Structure of Surfactant-Polyelcetrolyte Complexes*, Jawaharlal Nehru University, New Delhi (2003).

[5] P. Kekicheff and B. Cabane, *Acta Cryst*. **44**, 395 (1988).

[6] Y. Hendrikx, J. Charvolin, P. Kekichheff and M. Roth, *Liq. Cryst*. **2**, 677 (1987).

[7] P. O. Quist, B. Halle and I. Furo *J Chem. Phys*. **96**, 3875 (1992)

[8] M. C. Holmes, N. Boden,and K. Radley *Mol. Cryst. Liq. Cryst*. **100**, 93 (1983).

[9] M. C. Holmes *Curr. Opin. Colloid Interface Sci*. **3**, 485 (1998).

[10] M. Imai, A. Saeki, T. Teramoto, A. Kawaguchi, K. Nakaya, T. Kato and K. Ito *J. Chem. Phys*, **115**, 10525 (2001)

[11] C. E. Fairhurst, M. C. Holmes and M. S. Lever *Langmuir* **13**, 4964 (1997).

[12] S. S. Funari and G. Rapp *Proc. Natl. Acad. Sci. USA*, **96**, 7756 (1999).

[13] J. Burgoyne, M. C. Holmes and G. J. T. Tiddy *J. Phys. Chem*. **99**, 6054 (1995).

[14] S. S. Funari, M. C. Holmes and G. J. T. Tiddy *J. Phys. Chem* , **96**, 11029 (1992).

[15] P. Kekicheff and G. J. T. Tiddy *J. Phys. Chem.*, **93**, 2520 (1989).

[16] S. Puntambekar, M. C. Holmes and M. S. Lever *Liq. Cryst.* **27**, 743 (2002).

[17] R. Oda, J. Narayanan, P. A. Hassan, C. Manohar, R. A Salkar, F. Kern and S. J. Candau *Langmuir* **14**, 4364 (1998).

[18] M. S. Leaver, A. Fogden, M. C. Holmes and C. E. Fairhurst *Langmuir* **17**, 35 (2001).

[19] J. Israelachvili *Intermolecular and Surface Forces*, 2nd edition, Academic Press, London (1991).

[20] K. M. McGrath *Langmuir* **11**, 1835 (1995).

[21] F. Reiss-Husson and V. Luzzati *J. Phys. Chem.* **68**, 3504 (1964) .

[22] F. Husson, H. Mustacchi and V. Luzzati, *Acta Cryst.*, **13**, 668 (1960).

[23] T. Hashimoto, S. Koizumi and H. Hasegawa, *Macromolecules*, **25**, 1433 (1992) .